

Branching ratio change in K^- absorption at rest and the nature of the $\Lambda(1405)^*$

Akira Ohnishi^{1,2†}, Yasushi Nara^{1,3‡}, and Volker Koch^{2§}

1. *Division of Physics, Graduate School of Science, Hokkaido University, Sapporo 060, Japan*

2. *Nuclear Science Division, Lawrence Berkeley National Laboratory,
University of California, Berkeley, California 94720*

3. *Advanced Science Research Center, Japan Atomic Energy Research Institute,
Tokai, Ibaraki 319-11, Japan*
(December 3, 2017)

We investigate in-medium corrections to the branching ratio in K^- absorption at rest and their effect on the charged pion π^\pm spectrum. The in-medium corrections are due to Pauli blocking, which arises if the $\Lambda(1405)$ is assumed to be a \bar{K} -nucleon bound state and leads to a density and momentum dependent mass shift of the $\Lambda(1405)$. Requiring that the optical potential as well as the branching ratio are derived from the same elementary T -matrix, we find that the in-medium corrected, density dependent T -matrix gives a better description of the K^- absorption reaction than the free, density-independent one. This result suggests that the dominant component of the $\Lambda(1405)$ wave function is the $\bar{K}N$ bound state.

PACS numbers: 13.75.Jz, 25.80.Nv, 14.20.Jn, 36.10.Gv

I. INTRODUCTION

The problems of the low-energy K^-N interaction are longstanding. It is well known that the s-wave K^-N scattering length is repulsive at threshold [1] ($a_{K^-N} = -0.15$ fm), and a recent experiment clearly showed that the energy shift of the 1s atomic orbit of kaonic hydrogen is positive (i.e. K^-p interaction is repulsive) [2,3]. However, from a theoretical point of view it is more natural that the basic K^-N interaction is attractive. For instance, the leading order (Weinberg-Tomazawa-type) term in the chiral expansion is attractive for the K^-N channel.

If the s-wave, isospin $I = 0$ $\Lambda(1405)$ resonance is a bound state of $\bar{K}N$ [4,5], it is possible that the actual K^-p interaction is attractive although it appears repulsive in the scattering length and the energy shift of the kaonic hydrogen. This $\Lambda(1405)$ resonance is clearly seen in $K^-p \rightarrow \Sigma\pi$ reactions, and couples strongly to the K^-p channel. Since this $\Lambda(1405)$ lies just below the K^-p threshold, scattering through this resonance gives rise to a repulsive contribution to the scattering amplitude at threshold. This effect is readily understood by analogy to the proton-neutron (pn) scattering; the interaction between pn is attractive, but the scattering length in the deuteron channel ($I = 0, S = 1$) is repulsive, due to the existence of the deuteron as a bound state. In nuclear matter, however, the deuteron disappears, largely due to Pauli blocking, and the true attractive nature of the pn

interaction emerges. Similarly, the nature of the $\Lambda(1405)$ — a continuum bound state of $\bar{K}N$ or a genuine 3-quark state — can be studied by investigating the properties of the $\Lambda(1405)$ in nuclear matter since only the bound state component will be subject to Pauli-corrections.

One of the in-medium corrections suggested in the bound state picture is the mass shift of $\Lambda(1405)$ and the resulting density dependence of the real part of the K^- optical potential in nuclear matter, as extracted from the analysis of kaonic atoms [6]. There one finds that the optical potential changes sign — from repulsive to attractive — at rather low densities. In the bound state picture of $\Lambda(1405)$, this density dependence can be simply understood as the effect of the Pauli blocking of the proton inside the $\Lambda(1405)$, which leads to an upwards shift of the $\Lambda(1405)$ and thus to an attractive potential [7] (see also [8]), analogously to the deuteron and pn interaction in medium as described before. The resulting attractive K^- potential has interesting phenomenological consequences such as a possible condensate in neutron stars [9].

While the K^- optical potential is connected with the *diagonal* matrix element of the elementary T -matrix in the lowest order impulse approximation, the branching ratio from K^-N to $\pi\Lambda$ and $\pi\Sigma$ is given by the *off-diagonal* matrix element of the same T -matrix. Since the $I = 0$ amplitude ($\Lambda(1405)$ channel) interferes with that in the $I = 1$ channel [10], it is expected that the branching ratio changes considerably in the nuclear medium if the mass of the $\Lambda(1405)$ is shifted. This

* preprint HUPS-97-1, LBNL-40007

† e-mail: ohnishi@nucl.phys.hokudai.ac.jp

‡ e-mail: ynara@hadron03.tokai.jaeri.go.jp

§ e-mail: vkoch@nsdssd.lbl.gov

in-medium branching ratio correction should be seen in the particle (pair) multiplicities and in the pion spectra from K^- absorption reactions at rest on nuclear targets, ${}^A Z(K_{\text{stopped}}^-, \pi)$ [11–16], which contain various contributions of elementary processes, such as quasi free processes $K^- N \rightarrow Y \pi$, and the weak decay of hyperons $Y \rightarrow \pi N$. One of the pioneering work on the in-medium branching ratio can be seen in the analyses of the bubble chamber data [11]. An in-medium branching ratio for the primary interactions in ${}^{12}\text{C}$ has been extracted by counting several kinds of charged particle pairs observed in the bubble chamber. Although some assumptions went into this estimate, such as the conversion probability of Σ , the extracted branching ratios are clearly different from the free one. For example, the extracted in-medium branching ratio of the elementary process $K^- p \rightarrow \Sigma^+ \pi^-$ is much larger than that of $K^- p \rightarrow \Sigma^- \pi^+$, while the latter channel dominates in free space. In recent counter experiments, Outa et al. decomposed the experimental pion spectrum into the contributions from various elementary channels in ${}^4\text{He}(K_{\text{stopped}}^-, \pi^\pm)$ reactions by using the delayed time gate technique [12]. In the case of heavier targets such as ${}^{12}\text{C}$, however, it is very difficult to decompose π^\pm spectra in an unambiguous way solely based on experimental data. Therefore, Tamura et al. [15] obtained the spectral shapes of each contribution by carrying out a Monte Carlo simulation, which took account of Fermi-motion of nucleons and energy loss of hyperons in the target. The relative intensity of each component was then determined by fitting the sum of all contributions to the experimental data.

All these experimental data suggest the necessity of the in-medium branching ratio corrections, although the final state interactions make it difficult to extract the primary branching ratio. Thus, it is required to explain the experimental pion spectra themselves by means of theoretical models which take the in-medium corrections and multi-step interactions into account. In order to evaluate the final state multi-step interactions of the primary hyperon and pion, cascade type models [17–21] are considered to be the most reliable at present. In these models, each elementary two-body collision process is treated explicitly, which allows to include various multi-step processes.

The purpose of this paper is to elucidate the nature of $\Lambda(1405)$ resonance by analyzing the pion spectrum in K^- absorption reactions at rest on nuclei. We compare the calculated results based on two different scenarios of the $\Lambda(1405)$ resonance. The first scenario assume that the $\Lambda(1405)$ resonance is a genuine 3-quark state, and, hence, is not subject to Pauli blocking by nucleons in nuclei. In the second scenario, we assume that $\Lambda(1405)$ is a bound state of $\bar{K}N$, and the Pauli blocking of nucleons shifts the mass of $\Lambda(1405)$ upwards in nuclear medium. These two scenarios give different branching ratios and different absorption point distributions, as well. The first difference comes from the *off-diagonal* matrix elements. The difference in the absorption point distribution on the

other hand is due to a different K^- optical potential obtained in the bound state picture [7]. It is, thus, related to the *diagonal* elements of the T -matrix. The combined effects lead to significantly different pion spectra, especially in the (K^-, π^+) channel. After taking into account final state interactions of the produced hyperon and pion within the cascade model, it becomes possible to compare the calculated spectra with experimental data. From this comparison, we find that the interpretation of $\Lambda(1405)$ as a $\bar{K}N$ bound state gives a better description of K^- absorption reactions at rest.

The necessity of the branching ratio modification in ${}^A Z(K^-, \pi)$ reactions has already been pointed out in Refs. [22–25]. These proposed modifications come from the Fermi smearing and binding effects and thus essentially smear and shift both of the amplitudes in $I = 0$ and $I = 1$ channels in a similar way. On the other hand, since a mass shift of the $\Lambda(1405)$ only affects the $I = 0$ channel, we expect significant differences between the branching ratio calculated with only Fermi-smeared amplitudes and those where in addition the mass shift of the $\Lambda(1405)$ is taken into account. Actually, we will show that the branching ratio strongly depends on the scenario of $\Lambda(1405)$ in the case of K^- particle absorption at rest on ${}^{12}\text{C}$.

The scenarios considered here, pure bound state on the one hand or pure three-quark state on the other, are of course extreme. Most likely, the $\Lambda(1405)$ will be a superposition of both. However, our results suggest that the dominant component of the wave function of the $\Lambda(1405)$ indeed is the $K^- p$ bound state. Typically in models which take such an admixture into account, the *bare* $\Lambda(1405)$ state has a mass much higher than 1405 MeV and it is the coupling to the $K^- p$ state which brings the mass down to the correct value [26,27]. In medium, these $K^- p$ states are also Pauli blocked leading again to an upwards mass shift of the $\Lambda(1405)$. Taking the mass of the bare $\Lambda(1405)$ to infinity in this approach would correspond the extreme bound state picture presented here.

Throughout this paper, we assume that the in-medium corrections to the $I = 1$ amplitude are negligible.

II. THE MODEL OF $\Lambda(1405)$

In this section, we briefly summarize the description of $\Lambda(1405)$ as a bound state of $\bar{K}N$, and its modification in nuclear medium. We follow the treatment of Ref. [7].

We consider two $I = 0$ channels, $\bar{K}N$ and $\pi\Sigma$, to describe the $\Lambda(1405)$ resonance. Restricting ourselves to a non-relativistic treatment of the problem, the mass and width of the $\Lambda(1405)$ is obtained from the solution of the coupled channel Schrödinger equation,

$$\nabla^2 \psi_i(r) + k_i^2 \psi_i(r) - 2\mu_i \int V_{i,j}(r, r') \psi_j(r') d^3 r' = 0, \quad (1)$$

where $\psi_i(r)$ represents the relative wave function, μ_i is the reduced mass, and k_i is the momentum in the center of mass system for the channel $i = 1(\bar{K}N), 2(\pi\Sigma)$. Using a separable potential, the expression of the T -matrix is

$$V_{i,j}(k, k') = g^2 C_{i,j} v_i(k) v_j(k') = \frac{g^2}{\Lambda^2} C_{i,j} \Theta(\Lambda^2 - k^2) \Theta(\Lambda^2 - k'^2), \quad (2)$$

$$T_{i,j}(k, k', E) = g^2 v_i(k) v_j(k') [(1 - C \cdot G(E))^{-1} \cdot C]_{i,j}. \quad (3)$$

The propagator matrix G is given by

$$G_{i,j} = \text{diag}(g_i) = \delta_{ij} g_i, \quad (4)$$

$$g_i(E) = g^2 \int \frac{d^3 p}{(2\pi)^3} \frac{v_i^2(p)}{E - m_i - M_i - p^2/(2\mu_i)} = \frac{1}{2\pi^2} \frac{g^2}{\Lambda^2} \int_0^\Lambda \frac{p^2 dp}{E - m_i - M_i - p^2/(2\mu_i)}. \quad (5)$$

The scattering amplitude is directly related to the T -matrix by [28]

$$f_{i,j}(k, k') = -\frac{\sqrt{\mu_i \mu_j}}{2\pi} T_{i,j}(k, k'). \quad (6)$$

Finally, for the coupling matrix C_{ij} , we use the standard result derived from the $SU(3)$ flavor symmetry (see e.g. Refs. [4,5])

$$C_{i,j} = \begin{pmatrix} \bar{K}N & \pi\Sigma \\ -\frac{3}{2} & -\frac{\sqrt{6}}{4} \\ -\frac{\sqrt{6}}{4} & -2 \end{pmatrix} \begin{pmatrix} \bar{K}N \\ \pi\Sigma \end{pmatrix}. \quad (7)$$

By choosing the parameters Λ and g appropriately, the scattering amplitude extracted from experimental data by Martin [1] can be reproduced (see [7] for details). In this paper, we have used the parameters $\Lambda = 0.78$ GeV and $g^2 = 17.9$, which are taken from [7].

In the momentum space representation, the effect of the Pauli blocking can be readily included. In the nuclear medium, the intermediate proton states with momenta $p \leq k_f$ are forbidden, where k_f is the Fermi momentum, which changes the propagator in the $\bar{K}N$ channel to,

$$g_1(E, k_f) = \frac{g^2}{\Lambda^2} \int_0^\Lambda \frac{d^3 p}{(2\pi)^3} \frac{\Theta(k_f - |\vec{p} + M_N \vec{v}_\Lambda|)}{E - m_K - M_N - p^2/(2\mu_{Kp})}, \quad (8)$$

while that for the $\pi\Sigma$ channel remains unaffected. Note that we also include the dependence of the $\Lambda(1405)$ momentum. In Ref. [7] only the $\Lambda(1405)$ at rest has been considered. If, as suggested in [7], the Pauli blocking is responsible for the mass shift of the $\Lambda(1405)$, one should expect that for a given density this mass shift should become small once the momentum of the $\Lambda(1405)$ is large compared to the Fermi-momentum. In this case the momentum distribution of the $\Lambda(1405)$ -wave function has very little overlap with other nucleons in the matter and the effect of the Pauli-blocking becomes small.

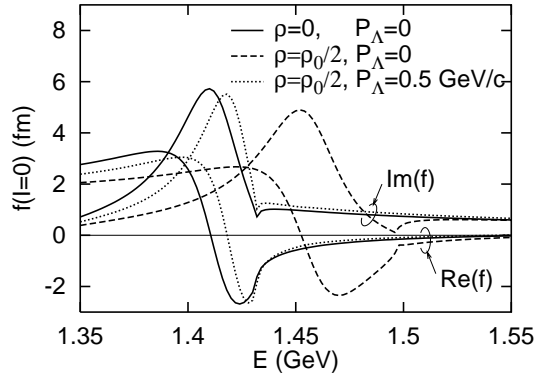


FIG. 1. Scattering Amplitude of $\bar{K}N$ in Nuclear Medium. Energy dependence of the scattering amplitude in $I = 0, \bar{K}N$ channel. Solid, dashed, and dotted lines show the calculated results at $(\rho, P_\Lambda) = (0, 0)$, $(\rho_0/2, 0)$, and $(\rho_0/2, 0.5 \text{ GeV}/c)$, respectively.

This is demonstrated in Fig. 1. There, we show the energy dependence of the calculated scattering amplitude under the three typical conditions, $(\rho, P_\Lambda) = (0, 0)$, $(\rho_0/2, 0)$, and $(\rho_0/2, 0.5 \text{ GeV}/c)$. At finite density with the $\Lambda(1405)$ at rest, the mean resonance mass (around the peak position of the imaginary part) shifts upward compared with that in free space. However, once the momentum of $\Lambda(1405)$ is large compared with the nuclear Fermi momentum, the effect of the Pauli blocking decreases and the mass shift is hardly seen. Therefore, a rather unique signature of the bound state picture of the $\Lambda(1405)$ is a density dependent upwards mass shift which should become smaller as the momentum of the $\Lambda(1405)$ increases with respect to the matter restframe. We are presently investigating to which extent this density *and* momentum dependent mass shift can be extracted experimentally by choosing appropriate kinematic conditions in (γ, K^+) , (π, K^+) and possibly (K^-, π) reactions [29].

III. STOPPED K^- REACTION

The mass shift of $\Lambda(1405)$ described above is expected to appear most clearly if it is created in the nuclear medium with a small momentum. The K^- absorption at rest is one possibility, and another possibility is to use (K^-, π) reaction at the magic momentum of $\Lambda(1405)$ at which the $\Lambda(1405)$ momentum becomes zero when pions are detected at forward angles.

In this paper, we focus our attention to the K^- absorption reaction at rest. For this reaction, the experimental charged pion spectra are available for several nuclear targets. The $\Lambda(1405)$ mass shift moves the $I = 0$ amplitude upwards in energy but does not affect the $I = 1$ amplitude. It, therefore, modifies the relative phase and strength of $I = 0$ and $I = 1$ amplitudes leading to different branching ratios for the reactions

$K^-p \rightarrow \pi^0\Lambda, \pi^-\Sigma^+, \pi^0\Sigma^0, \pi^+\Sigma^-$, as compared to the free ones.

A. Branching ratio

In Fig. 2, we show the model dependence of the calculated branching ratio. In this figure, we compare the results of the following models or parameterizations: M: Martin's parameterization in free space (without Fermi smearing). MF: Martin's parameterization in nuclei, with Fermi smearing and binding energy correction. Binding energies are chosen as $B = 12.5$ MeV (MFa) [30] and $B = 17.34$ MeV (MFb). The latter value corresponds to the neutron separation energy of ^{12}C . KF: Koch's amplitude with Fermi smearing, and averaged over density according to the absorption probability. The binding energy correction is ignored in the case of KF, but the calculated pion spectra are not very sensitive to this binding energy correction, once the mass shift of $\Lambda(1405)$ is included. The density dependence of the branching ratio is also shown in the case of Koch's amplitude. The momentum distribution used here has the Gaussian form, and assumed to be independent on the position. The same momentum distribution is adopted in all the above calculations.

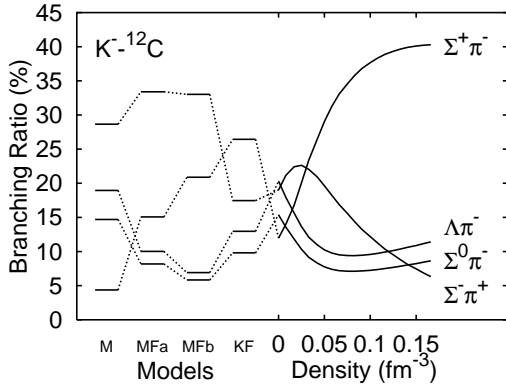


FIG. 2. Model dependence of the branching ratio. Branching ratios with models MFa, MFb are calculated through the Fermi smeared T -matrix with binding energy correction, which is density independent. In the case of model KF, we show the density dependence of the branching ratios (right solid curves) and their average based on the probability distribution shown in Fig. 4.

It is clear that, in the case of KF, the process of $K^-p \rightarrow \Sigma^+\pi^-$ is strongly enhanced if the density is high, while the quasi-free π^+ production ($K^-p \rightarrow \Sigma^-\pi^+$) is suppressed. As a result, in the above two channels the density averaged branching ratios in KF largely differ from those in MF.

At a glance, the above difference looks too large, since the K^- absorption is considered to occur only at the

nuclear surface region, and therefore, the branching ratio in the low-density region governs the total (position averaged) ratio. However, the two models also lead to quite different K^- optical potentials, and consequently to different absorption point distributions. In order to illustrate this point, we show the K^- optical potential and the absorption point distribution in the next two figures. In Fig. 3, we show the K^- optical potential for the two models, MFb and KF, which have been obtained in the lowest order impulse approximation

$$U(r) = -\frac{2\pi\hbar^2}{\mu} \left(1 + \frac{\mu}{m_N} \right) \times \langle K^-N|T(\rho(r))|K^-N \rangle_{pn} \rho(r) + U_{Coulomb}(r) . \quad (9)$$

As has been already pointed out by Koch [7], the optical potential of KF has a strong density dependence in accordance with the analysis of kaonic atoms [6]. For example, while the K^-N real potential is repulsive at low densities, it turns attractive at a finite nucleon density ($\rho \geq 0.25\rho_0$). As a result, the K^- wave function is pulled inside, towards higher densities. This is contrary to the straightforward impulse approximation based on the free T -matrix, which is repulsive in Martin's parameterization. Consequently, in this case the K^- wave function is pushed away from the nucleus and lower densities are being probed.

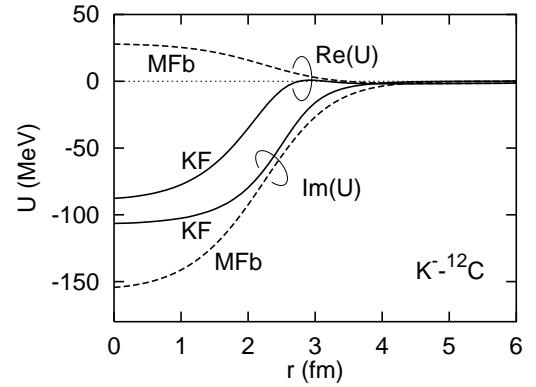


FIG. 3. Optical potential U between K^- and ^{12}C . Dashed and solid lines represent the potential calculated with models of MFb and KF, respectively. We have used the lowest order impulse approximation Eq. (9).

This difference in the radial distribution for the K^- -wave function is shown in Fig. 4 where the calculated absorption point distribution of K^- on ^{12}C is shown. The absorption probability is assumed to be proportional to the imaginary part of the optical potential and the wave function squared,

$$\frac{dP_{abs}}{dr} \propto -\text{Im}(U(r)) |\psi(r)|^2 , \quad (10)$$

where $\psi(r)$ is the solution of the Schrödinger equation under the potential U . (We have assumed that K^- is absorbed from a p -orbit [31].)

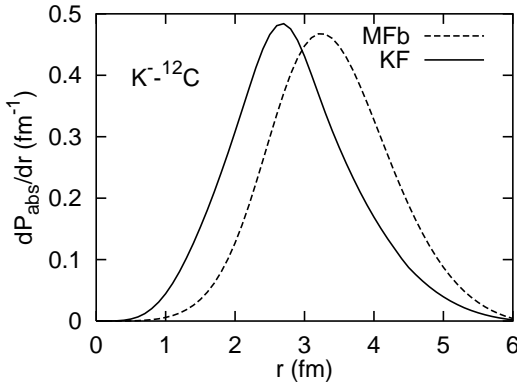


FIG. 4. Absorption point distribution of K^- on ^{12}C . Dashed and solid lines represent the calculated results with models of MFa and KF, respectively. The absorption probability is assumed to be proportional to $-Im(U)|\psi(r)|^2$, where $\psi(r)$ is the solution of the Schrödinger equation with the optical potential U .

The calculated average branching ratio can be compared with the one extracted from experimental data [11], although there are some assumptions in their estimate, such as the conversion probability of Σ . Obviously the model KF gives values closer to the experimental estimates than models MFa and MFb in the $I = 0$ ($\Sigma\pi$) channels. Especially, the model KF explains the inversion of the branching ratios of $K^-p \rightarrow \Sigma^+\pi^-$ and $\Sigma^+\pi^-$ from free values.

TABLE I. Average branching ratio in K^- absorption at rest on ^{12}C . Branching ratios in models of M, MFa, MFb, KF are shown in comparison with the experimentally estimated one [11].

	M	MFa	MFb	KF	Exp.
$K^-p \rightarrow \Lambda\pi^0$	9.5	5.0	3.5	6.5	4.4
$K^-n \rightarrow \Lambda\pi^-$	18.9	10.0	6.9	13.0	8.7
$K^-p \rightarrow \Sigma^-\pi^+$	28.7	33.4	33.0	17.5	16.8
$K^-p \rightarrow \Sigma^0\pi^0$	9.2	20.1	24.0	17.0	25.7
$K^-p \rightarrow \Sigma^+\pi^-$	4.4	15.1	20.9	26.4	37.7
$K^-n \rightarrow \Sigma^-\pi^0$	14.7	8.2	5.8	9.8	3.3
$K^-n \rightarrow \Sigma^0\pi^-$	14.7	8.2	5.8	9.8	3.3

B. π^- spectrum

In order to calculate the resulting π^- spectra we have carried out a simple Monte-Carlo simulation of K^- absorption reaction at rest on ^{12}C . This simulation includes (a) absorption point distribution shown in Fig. 4, (b) branching ratio shown in Fig. 2, (c) multiple scattering

of the produced pion and hyperon, (d) Σ conversion to Λ , and (e) real part of the optical (mean field) potential for Λ and Σ . We have assumed that πN scattering occurs through the Δ formation, and the pion true absorption is described by $\Delta N \rightarrow NN$. The scattering and Σ conversion cross sections are calculated with Nijmegen model D potential [32]. The hyperon-nucleus potential is assumed to have the form

$$U_Y = \alpha_Y \frac{U_N(\rho)}{|U_N(\rho_0)|}, \quad U_N = \alpha \left(\frac{\rho}{\rho_0} \right) + \beta \left(\frac{\rho}{\rho_0} \right)^\gamma, \quad (11)$$

$$\alpha = -124 \text{ MeV}, \beta = 70.5 \text{ MeV}, \gamma = 2. \quad (12)$$

The factor $\alpha_\Lambda = 30$ MeV is chosen to reproduce the depth of -30 MeV for Λ in nuclear matter. For Σ , we chose $\alpha_\Sigma = 10$ MeV. The collisions between the produced pion and hyperon are ignored.

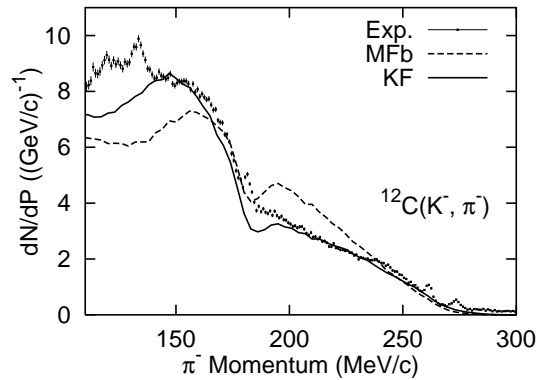


FIG. 5. π^- momentum spectrum from K^- absorption at rest on ^{12}C . Dashed and solid lines show the calculated results with models MFb and KF, respectively. Experimental data (point with error bar) is taken from [13]. Since the absolute values are not shown in [13], we have assumed that $dN/dp|_{\text{exp.}}((\text{GeV}/\text{c})^{-1}) = \text{Count/bin}|_{\text{exp.}}/800$.

In Fig. 5, we show the momentum spectrum of π^- in $^{12}\text{C}(\text{stopped } K^-, \pi^-)$ reaction. The individual contributions are shown in Fig. 6. The highest momentum component comes from the quasi-free Λ production, the component at around 185 MeV/c comes from the weak decay of Σ^- particles, the largest peak at around 160 MeV/c is due to quasi-free Σ production ($K^-p \rightarrow \pi^-\Sigma^+$, $K^-n \rightarrow \pi^-\Sigma^0$), and the lowest momentum component comes from the weak Λ decay. The last component (Λ decay) includes the Σ conversion and the Σ^0 electromagnetic decay component ($\Sigma^0 \rightarrow \gamma\Lambda$). All of these yields well agree with the estimate by Tamura et al. [13].

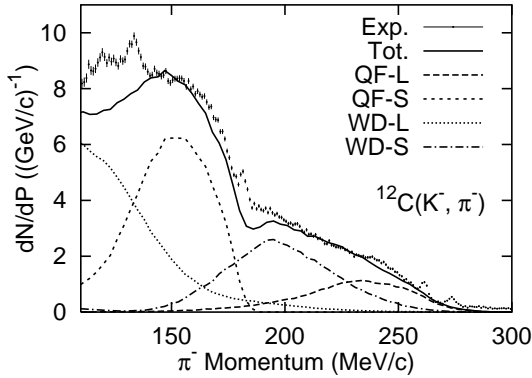


FIG. 6. Components in π^- momentum spectrum from K^- absorption at rest on ^{12}C . Component dissolution of π^- spectrum shown in Fig. 5 in the model KF. Experimental data (point with error bar) is taken from [13]. Solid line represents the total yield. Long and short dashed lines show quasi-free Λ and Σ productions, respectively. Dotted and dot-dashed lines show the contributions of Λ and Σ weak decays, respectively. It is noteworthy that the Λ weak decay component includes Σ^0 sequential decay and other Σ conversion, thus it has a longer tail in high momentum region compared with the estimate of Ref. [13].

From Fig. 5, we see the suppression of the Σ^- weak component and the enhancement of the quasi-free Σ production component in KF compared with the results of MFb. This is mainly due to the branching ratio change in the model KF. In addition, since the absorption is assumed to occur only at the surface region in the model MFb, Σ conversion is estimated to be smaller. As a result, the model KF agrees better with the experimental data by Tamura et al. [13].

C. π^+ spectrum

Since the largest difference in the branching ratio can be seen in the double charge exchange reaction $K^-p \rightarrow \pi^+\Sigma^-$ (see Fig. 2), a comparison with the π^+ spectrum should be more sensitive to the proposed in-medium effect. Although the quasi-free Σ production part of this double charge exchange reaction is well analyzed by using direct reaction theories, the weak decay component of Σ^+ has been neglected as a *background*. Actually, it contains the weak decay of the Σ^+ particles with various velocities; some of them stop in the emulsion (the peak at around 185 MeV/c) and the rest decay during the slowing down process. Thus the interpretation of the spectrum is very complicated, and the extraction of the initial momentum distribution of Σ^+ particles is difficult. However, we expect that the total yield of Σ^+ decay is a rather robust observable. To demonstrate this, we have attempted to fit the experimental data [16], including the ‘background’ from the weak Σ^+ decay, by taking into account the following sources. We have assumed that the

weak decay spectra of stopped and moving Σ^+ centered at 185 MeV/c have a Lorenzian and two-range Gaussian form, respectively. The π^+ free production on hydrogen at 173 MeV/c is assumed to be a Lorenzian, and a Breit-Wigner type spectrum with threshold correction is used to fit the quasi-free part on ^{12}C . The charge exchange reactions such as $K^-N \rightarrow \pi\Lambda$ followed by $\pi N \rightarrow \pi^+N'$ are ignored in the fitting procedure, since their contributions are negligible. The resulting fit is shown in Fig. 7.

By using this fit, we can reconstruct the π^+ spectrum from the K^- absorption on ^{12}C , where the subsequent atomic processes such as slowing down of Σ^+ are removed. For this reconstruction, the following free branching ratios are used; $K^-p \rightarrow \pi^-\Sigma^+(4.37\%)$, $\pi^+\Sigma^-(28.66\%)$ and $\Sigma^+ \rightarrow \pi^+n(48.3\%)$. In addition, the Σ^+ weak decay spectrum without the subsequent atomic processes is assumed to have the same shape as the fitted moving Σ^+ spectrum. In Fig. 8, we show the calculated π^+ spectra with this reconstructed data. We have adjusted the scale of this reconstructed data by requiring that its weak decay tail agrees with the calculated results approximately, then the difference at the quasi-free part becomes significant: The yield of the quasi-free component in the model MFb is larger by about a factor of two than that in the model KF.

This difference mainly comes from the branching ratio difference in the $K^-p \rightarrow \pi^+\Sigma^-$ channel. The absolute value of the Σ^+ particles which decay outside of the nucleus is similar in the two models, because the reaction occurs at the surface in the model MFb and Σ^+ particle can easily escape from nuclei. However, the relative yield of Σ^+ particles as compared to the quasifree peak, which essentially is the ratio of Σ^+/Σ^- , differs by more than a factor of two.

In order to make a clear comparison, we have extracted an approximate value for the branching ratio, by taking the ratio of the contribution to the quasi-free bump to the sum of moving Σ^+ and Σ^+ at rest. This can then be directly compared with the results from the different models (see Table II). Clearly, the model based on the K^-p -bound state for the $\Lambda(1405)$ compares best with our estimate of the branching ratio from experiment. It is still 50 % off, though, but as compared to the free space value or that including Fermi smearing, it constitutes a significant improvement.

The remaining difference may very well be due to the interaction between Σ and the residual nuclei, $^{11}\text{B}^*$, which can have a structure $\alpha + \alpha + t$. It is well known that the ΣN interaction has a strong spin-isospin dependence, and there is a large uncertainty in its strength. In addition, when resonance states or unstable bound states such as ^4He are created in the subsystem, the Σ conversion probability as well as the initial branching ratio may be modified from the present estimate. All of these effects are ignored in this work, and should be included in future works, once they are reasonably well controlled.

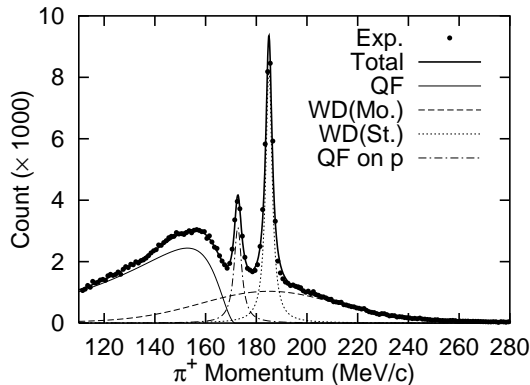


FIG. 7. The fitted spectrum to $^{12}\text{C}(K_{\text{stopped}}^-, \pi^+)$ data in Ref. [16]. The thick solid curve show the fitted total spectrum to the experimental data shown by dots. The sharp peak at around 185 MeV/c comes from the weak decay of Σ^+ which stopped in the scintillator (fitted by the dotted curve), and that at around 172 MeV/c corresponds to the free π^+ production on the protons in the plastic scintillator, $K^- p \rightarrow \Sigma^- \pi^+$ (dash-dotted curve). The thin solid and dashed curves show the contribution from quasi-free π^+ production on ^{12}C and weak decay of moving Σ^+ , respectively.

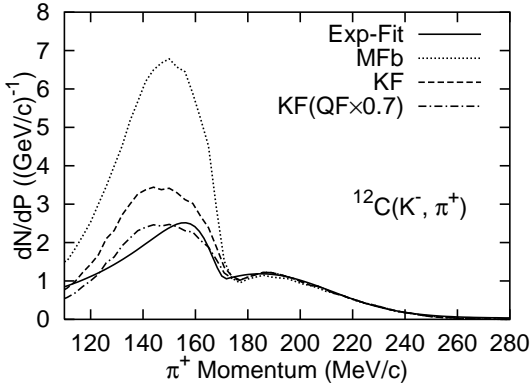


FIG. 8. π^+ momentum spectrum from K^- absorption at rest on ^{12}C . Dotted and dashed lines show the calculated results with models MFb and KF, respectively. Our fitting result to the experimental data [16] is shown by the solid curve. We have chosen the normalization factor $dN/dp|_{\text{exp.}}((\text{GeV}/c)^{-1}) = \text{Count}/\text{bin}|_{\text{exp.}}/1300$, by requiring that the calculated weak decay tails agree with the fitting result to the experimental data. This normalization factor corresponds to the number of experimentally detected events of 1.3×10^6 . The dash-dotted line shows the modified calculated results of model KF, with a reduction factor 0.7 for quasi-free π^+ .

TABLE II. Extracted multiplicity of escaped quasi-free π^+ and Σ^+ particles. Multiplicities in model M, MFb, and KF are compared with those estimated from the experimental data. In the models MFb and KF, effects of π rescattering and absorption as well as Σ conversion are included within the Monte-Carlo simulation used in this work. We have assumed that the number of events is 1.3×10^6 in the experiment.

	M	MFb	KF	Exp.	(Counts)
QF π^+ (A)	0.287	0.298	0.153	0.103	(1.33×10^5)
Σ^+ (B)	0.044	0.137	0.143	0.184	(2.40×10^5)
Ratio (A/B)	6.558	2.180	1.075	0.554	

IV. SUMMARY AND OUTLOOK

In this paper, we consider two extreme pictures of the $\Lambda(1405)$ and their consequences for stopped K^- experiments. The first scenario assumes that $\Lambda(1405)$ is a three-quark state, rather than a bound state of $\bar{K}N$. In this case it will not be subject to Pauli blocking in the nuclear medium, and the matrix elements such as $K^- N \rightarrow \pi \Sigma$ are density independent. In the other scenario, we have assumed that $\Lambda(1405)$ is a bound state of $\bar{K}N$ and, thus, is subject to Pauli-blocking in the medium. While the full, Pauli corrected T -matrix has been used in the calculations, the dominant effect is a density and momentum dependent mass shift of the $\Lambda(1405)$. This mass shift modifies the relative phase and relative strength between the matrix element of $I = 0$ and $I = 1$ channels, and leads to a change of the branching ratio. It also affects the potential between K^- and the target nucleus, and as a result, K^- absorption can occur deeply inside the nucleus in the latter scenario.

We have simulated the K^- absorption reaction at rest on ^{12}C nucleus by combining these results. The largest difference between the results of two scenarios can be found in the ratio $\Sigma^+ \pi^- / \Sigma^- \pi^+$. In the bound state picture, the first channel is enhanced at finite densities by the interference of $I = 0$ and $I = 1$ amplitudes. This difference appears most clearly in the π^+ spectrum. The experimental data [16] suggest that the escaping Σ^+ particle is more abundant than π^+ particles produced in the quasi-free process, $K^- p \rightarrow \Sigma^- \pi^+$. The comparison of the calculated results of π^- and π^+ spectra with the experimental data [13,16] suggests that the latter scenario — the $\Lambda(1405)$ is a bound state of $\bar{K}N$ — gives a better description of this reaction, due to the enhancement of $K^- p \rightarrow \Sigma^+ \pi^-$ branching ratio. Therefore, we conclude that the dominant component of the $\Lambda(1405)$ wave function is the $\bar{K}N$ bound state.

The above conclusion is, however, only an in-direct support of the latter scenario, since the change in the branching ratio is mostly due to the mass shift of the $\Lambda(1405)$. Such a mass shift could for instance also be

due to simple mean field effects. Also, it would be of course preferable if one could observe the mass shift directly. The in-medium effect which is more unique to the bound state picture is the momentum dependence of the mass shift of the $\Lambda(1405)$; if the $\Lambda(1405)$ momentum is larger than the nuclear Fermi momentum, the effects of the Pauli blocking is reduced, and the mass shift disappears. Therefore, the best confirmation for the bound state picture of the $\Lambda(1405)$ will be the observation of both the momentum and density dependence of its mass shift, by comparing two kind of reactions — the first involves "fast" $\Lambda(1405)$ particles at finite nuclear densities, and in the second type of reactions, $\Lambda(1405)$ particles are produced at very small momenta. As for the second type of reactions, it is the most ideal to use the magic momentum of $\Lambda(1405)$ in (K^-, π^-) reaction. This reaction can be used for the first, too, when π^- particle is detected at relatively large angles. The work on this line is in progress [29].

The authors would like to thank Dr. H. Tamura, Dr. H. Outa, Professor T. Harada, Professor K. Yazaki, Mr. T. Koike, Dr. J. Schaffner and Dr. M. Arima for fruitful discussions. This work was supported in part by the Japan Society for Promotion of Science, the Grant-in-Aid for Scientific Research (Nos. 07640365 and 09640329) and the Overseas Research Fellowship from the Ministry of Education, Science and Culture, Japan, and by the Director, Office of Energy Research, Office of High Energy and Nuclear Physics, Nuclear Physics Division of the U.S. Department of Energy under Contract No. DE-AC03-76SF00098. Two of the authors (A.O. and Y.N.) also thank the members of nuclear theory group for their hospitality during the stay at LBNL.

- [1] A. D. Martin, Nucl. Phys. **B179**, 33 (1981).
- [2] T. M. Ito, Ph.D. thesis, Univ. of Tokyo, 1996.
- [3] M. Iwasaki et al., Phys. Rev. Lett. **78**, 3067 (1997).
- [4] R. H. Dalitz, T. C. Wong, and G. Rajasekaran, Phys. Rev. **153**, 1617 (1967).
- [5] P. B. Siegel and W. Weise, Phys. Rev. **C38**, 2221 (1988).

- [6] E. Friedman, A. Gal, and C. J. Batty, Phys. Lett. **B308**, 6 (1993).
- [7] V. Koch, Phys. Lett. **B337**, 7 (1994).
- [8] T. Waas, N. Kaiser, and W. Weise, Phys. Lett. **B365**, 12 (1996).
- [9] G. E. Brown, H. Lee C, M. Rho, and V. Thorsson, Nucl. Phys. **A567**, 937 (1994).
- [10] R. H. Dalitz and S. F. Tuan, Ann. Phys. (NY) **3**, 307 (1960).
- [11] C. Vander Velde-Wilquet et al., Nuovo Cimento **39A**, 538 (1977).
- [12] H. Outa, T. Yamazaki, M. Iwasaki, and R. S. Hayano, Prog. Thero. Phys. Suppl. **117**, 177 (1994).
- [13] H. Tamura et al., Phys. Rev. **C40**, R479 (1989).
- [14] H. Tamura et al., Nucl. Phys. **A479**, 161c (1988).
- [15] H. Tamura, R. S. Hayano, H. Outa, and T. Yamazaki, Prog. Theor. Phys. Suppl. **117**, 1 (1994).
- [16] K. Kubota et al., Nucl. Phys. **A602**, 327 (1996).
- [17] Y. Yariv and Z. Frankel, Phys. Rev. **C20**, 2227 (1979).
- [18] J. Cugnon, T. Mizutani, and J. Vandermeulen, Nucl. Phys. **A352**, 505 (1981).
- [19] G. F. Bertsch and S. Das Gupta, Phys. Rep. **160**, 189 (1988).
- [20] W. Cassing, V. Metag, U. Mosel, and K. Niita, Phys. Rep. **188**, 363 (1990).
- [21] Y. Nara, A. Ohnishi, T. Harada, and A. Engel, Nucl. Phys. **A614**, 433 (1997).
- [22] C. B. Dover, D. J. Millener, and A. Gal, Phys. Rep. **184**, 1 (1989).
- [23] T. Harada and Y. Akaishi, Prog. Theor. Phys. **96**, 145 (1996).
- [24] A. S. Rosenthal and F. Tabakin, Phys. Rev. **C22**, 711 (1980).
- [25] W. A. Bardeen and E. W. Torigoe, Phys. Rev. **C3**, 1785 (1971).
- [26] K. Masutani, Nucl. Phys. **A483**, 565 (1988).
- [27] T. Hamaie, M. Arima, and K. Masutani, Nucl. Phys. **A591**, 675 (1995).
- [28] J. M. Eisenberg and D. S. Koltun, *Theory of Meson Interactions with Nuclei* (J. Wiley & Sons, New York, 1980).
- [29] V. Koch and A. Ohnishi, in preparation .
- [30] Y. Nara, A. Ohnishi, and T. Harada, Phys. Lett. **B346**, 217 (1995).
- [31] T. Koike, Private Communication (1996).
- [32] M. M. Nagels, T. A. Rijken, and J. J. de Swart, Phys. Rev. **D15**, 2547 (1977).